Available online at www.sciencedirect.com

ScienceDirect

Procedia Engineering 4 (2010) 263–271

Procedia Engineering

www.elsevier.com/locate/procedia

ISAB-2010

Fluid-structure interaction of submerged floating tunnel in wave field

Fei Ge*, Wei Lu, Xiaodong Wu, Youshi Hong

State Key Laboratory of Nonlinear Mechanics, Institute of Mechanics, Chinese Acedemy of Sciences, Beijing 100190, China

Received 18 July 2010; revised 2 August 2010; accepted 3 August 2010

Abstract

The aspect ratio of submerged floating tunnel (SFT), i.e. the ratio of length to diameter, is usually as large as 10^2 to 10^3, which means the behavior of SFT would like a slender cylinder restrained by tethers. Although SFT is usually placed under the water surface at a certain depth, surface wave has important influence on its dynamic response due to the slenderness. This paper performs analyses on the fluid-structure interaction of SFT in wave field. Potential fluid theory is adopted to describe the wave field. Boundary element method is used to solve the interaction between SFT and surface wave. Wave potential is divided into three parts, including incident wave potential, diffraction wave potential and radiation wave potential. SFT is discretized into finite elements and its dynamic response is finally solved in frequency domain. As a case study, the values of design parameters for SFT prototype in Qiandao Lake are adopted. Two different tunnel end connectors are used to compare the distributions of tunnel deflections, axial membrane forces at the tube segment connectors and tunnel end connectors.

Keywords: submerged floating tunnel; fluid-structure interaction; wave potential; boundary element method

1. Introduction

Submerged floating tunnel (SFT) is a potential choice as a traffic structure placed in straits, rivers, lakes and so on. Usually, SFT consists of many tube segments which are connected together. As a priority advantage compared to the traditional structures, such as cable-stayed bridge and underground tunnel, the cost per unit length of SFT does not increase with the increase of total span [1]. SFT may be the only choice when the span of crossing is large enough so that the traditional structures are impossible to be built.

Aspect ratio of SFT, which is defined as the ratio of span to characteristic length of tube cross-section, is usually as large as 10^2 to 10^3. It means that the dynamic behavior of SFT would like a slender beam restrained by tethers. Therefore, the interaction between SFT and surrounding fluid is significant. Here, due to the slenderness of SFT, the deformation of SFT under hydrodynamic loads composes different vibration modes. Thus, it is not appropriate to assume that SFT is rigid when we compute the fluid forces exerting on it.

* Corresponding author. Tel.: +86-10-82543968; fax: +86-10-62561284.
E-mail address: gefei@imech.ac.cn

1877-7058
doi:10.1016/j.proeng.2010.08.030

Although SFT is placed under the water surface at a certain depth, surface wave has important influence on its dynamic response due to the slenderness of structure. Moreover, the wave forces and dynamic response of SFT are coupled, which must be taken into account in the numerical simulation. In order to examine the fluid-structural interaction behavior of flexible structures, Wu [2], Price et al. [3], Bishop et al. [4] and Newman [5] presented a generalized three-dimensional hydroelasticity theory for a flexible body of arbitrary shape in wave fields. It adopts a frequency-domain approach by expanding the structural displacements and fluid velocity potential into structural mode components.

In this paper, a hydroelastic model of SFT is presented based on three-dimensional finite element model. Fluid-structural interaction is solved using boundary element method (BEM) [6]. The dynamic equation of SFT is solved in frequency-domain. As a case study, we adopt the design of submerged floating tunnel prototype (SFTP) at Qiandao Lake [7, 8]. The deflections of tunnel and the axial forces at connectors are presented and compared when using different tunnel end connectors.

2. Hydroelastic model

The equation of motion describing the response of a discretized structure to external excitation may be written as

$$\mathbf{M}\ddot{\mathbf{U}} + \mathbf{C}\dot{\mathbf{U}} + \mathbf{K}\mathbf{U} = \mathbf{F} \tag{1}$$

where $\mathbf{M}$, $\mathbf{C}$ and $\mathbf{K}$ denote mass, structural damping and stiffness matrices, respectively. The vectors $\mathbf{U}$, $\dot{\mathbf{U}}$ and $\ddot{\mathbf{U}}$ represent the structural displacements, velocities and accelerations, respectively, and the column vector $\mathbf{F}$ denotes the external forces.

For a finite element structure, the governing matrix equation of dry natural vibrations is

$$\left(-\omega^2\mathbf{M} + \mathbf{K}\right)\mathbf{d} = \mathbf{0} \tag{2}$$

where ω is dry natural frequency and $\mathbf{d}$ is dry natural mode. As a solution of the eigenvalue problem, ω and $\mathbf{d}$ in Eq. (2) are obtained for each ith dry mode, where i=1,2,…, N, N is the total number of degrees of freedom. Natural modes matrix $\mathbf{D}$ can be constituted

$$\mathbf{D} = \left[\mathbf{d}_1, \mathbf{d}_1, ..., \mathbf{d}_N\right] \tag{3}$$

The distortion of the structure may be expressed as the sum of the deflections in the natural modes,

$$\mathbf{U} = \mathbf{D}\mathbf{p}(t) \tag{4}$$

where $\mathbf{p}$ is the principle coordinates vector. By substituting Eq. (4) into Eq. (1) and pre-multiplying by $\mathbf{D}^{\mathrm{T}}$, the following generalized equation in terms of the principal coordinates of the structure is obtained

$$\mathbf{a}\ddot{\mathbf{p}}(t) + \mathbf{b}\dot{\mathbf{p}}(t) + \mathbf{c}\mathbf{p}(t) = \mathbf{Q}(t) \tag{5}$$

Here $\mathbf{a}$, $\mathbf{b}$ and $\mathbf{c}$ denote the generalized mass, structural damping and stiffness matrices, respectively, and are defined as

$$\mathbf{a} = \mathbf{D}^{\mathrm{T}}\mathbf{M}\mathbf{D}, \quad \mathbf{b} = \mathbf{D}^{\mathrm{T}}\mathbf{C}\mathbf{D}, \quad \mathbf{c} = \mathbf{D}^{\mathrm{T}}\mathbf{K}\mathbf{D}, \quad \mathbf{Q} = \mathbf{D}^{\mathrm{T}}\mathbf{F} \tag{6}$$

The generalized force matrix, $\mathbf{Q}(t)$ represents the fluid-structural interaction and all other external forces (e.g. wave forces, etc.).

The fluid is assumed to be inviscid, incompressible and its motion is irrotational. Therefore, the fluid velocity vector, $\mathbf{v}$, can be defined as the gradient of the velocity potential function ϕ as

$$\mathbf{v}(x,y,z,t) = \nabla\phi(x,y,z,t) \tag{7}$$

Velocity potential ϕ satisfies the Laplace equation and the given boundary values as

$$\nabla^2\phi = 0 \qquad \text{within fluid} \tag{8}$$

$$-\upsilon\phi + \partial\phi/\partial z = 0 \qquad \text{at free surface, } z = 0 \tag{9}$$

$$\partial\phi/\partial z = 0 \qquad \text{at sea floor, } z=-d \tag{10}$$

$$\partial\phi/\partial\mathbf{n} = \mathbf{V}\bullet\mathbf{n} \qquad \text{on wetted structural surface } S \tag{11}$$

where υ is the wave number, $\upsilon = \omega^2/g$, ω is the wave frequency, $\mathbf{V}$ is the velocity vector of structure at the wetted surface and $\mathbf{n}$ is the wetted surface normal vector. The z-axis coincides with the gravity acceleration and towards upward with its origin at the water surface and d is the water depth.

Furthermore, the total wave potential can be split into three parts [6] if linear wave theory is adopted:

$$\phi = \phi_{\mathrm{I}} + \phi_{\mathrm{D}} + \sum_{r=1}^{N} p_r(t)\phi_r(x,y,z) \tag{12}$$

Here ϕ_{I} is incident wave potential, ϕ_{D} is diffraction (or scattered) potential and ϕ_r is radiation potential which is produced by the structure motions and distortions with unit principal coordinate in each of the principle modes in an otherwise still water.

Assuming that the temporal variation of the principal coordinates is sinusoidal and has the form:

$$p_r(t) = p_r \exp(-i\omega t), \quad r \in N \tag{13}$$

The structure boundary condition [Eq. (11)] can be deduced for each potential:

$$\partial\phi_{\mathrm{D}}/\partial\mathbf{n} = -\partial\phi_{\mathrm{I}}/\partial\mathbf{n}, \quad \partial\phi_r/\partial\mathbf{n} = -i\omega\mathbf{d}_r\bullet\mathbf{n} \tag{14}$$

Moreover, the diffraction and radiation potentials should also satisfy the radiation condition at infinity.

Once the potentials are determined, the total linearised pressure can be found from Bernoulli's equation by integration over the structural wetted surface, that is:

$$p = i\omega\rho\phi - \rho g z \tag{15}$$

Substituting Eqs. (12) and (15) into the right hand side of Eq. (5) then subdividing the pressure into excitation and radiation parts:

$$F_r^W = i\omega\rho \iint_S \mathbf{n}^{\mathrm{T}}\mathbf{u}_r(\phi_{\mathrm{I}} + \phi_{\mathrm{D}})\,\mathrm{d}S \tag{16}$$

$$F_r^R = \sum_{k=1}^{N} p_k \left(\omega^2 A_{rk} - i\omega B_{rk}\right) \exp\left(-i\omega t\right) \tag{17}$$

$$A_{rk} = \frac{\rho}{\omega^2} \mathrm{Re} \int_S \mathbf{n}^{\mathrm{T}} \mathbf{u}_r \left(-i\omega\right) \phi_k \mathrm{d}S \tag{18}$$

$$B_{rk} = -\frac{\rho}{\omega} \mathrm{Im} \int_S \mathbf{n}^{\mathrm{T}} \mathbf{u}_r \left(-i\omega\right) \phi_k \mathrm{d}S \tag{19}$$

Here Re and Im denote the real and imaginary parts of a complex variable, respectively. Coefficients A_{rk} are in phase with the acceleration and act as additional mass. Coefficients B_{rk} are in phase with the velocity and appear as additional damping in Eq. (5). $\mathbf{u}_r$ is *r*th modal displacement at any point on the structure.

Now substituting Eqs. (13), (15), (16) and (17) into Eq. (5), the equation of principal coordinates can be rewritten as:

$$\left[-\omega^2 \left(\mathbf{a} + \mathbf{A}\right) - i\omega(\mathbf{b} - \mathbf{B}) + \mathbf{c}\right]\mathbf{p} = \mathbf{F} \tag{20}$$

where $\mathbf{A}$ is the added mass matrix, $\mathbf{B}$ is the hydrodynamic damping matrix and external force vector $\mathbf{F}$ contains the incident and diffraction wave forces, hydrostatic and gravity forces.

The solution of Eq. (20) gives the principal coordinates $\mathbf{p}$ and displacement of any point of the structure obtained by Eq. (4). To solve Eq. (20), we must get the value of radiation potential first. According to the boundary conditions (Eq. (14)), if the dry natural modes of the structure are known, the radiation potential can be deduced using the same method as the diffraction potential. Here Green function method and boundary element method (BEM) are adopted to solve the Laplace equation (Eq. (8)) with the boundary conditions (Eqs. (9-11)).

3. Hydroelasticity of SFTP

Fig. 1(a) shows the schematic diagram of submerged floating tunnel prototype (SFTP) at Qiandao Lake [7, 8]. It consists of 5 tube segments and the total length is 100m. The outer diameter of tube is 4.39m and the wall thickness is 0.42m. Cross-section of tube is a sandwich structure shown as Fig. 1(b), which consists of inner steel shell, outer aluminum shell and concrete shell in the middle for the aims of corrosion resistance, collision protection, tunnel weight balance, etc. The connections between tunnel and shores have the characteristics of hinge with a axial stress relaxation device applied at one tunnel end.

SFTP is submerged 4.2m under the water. The average water depth is 17.28m. The design wave height is 1m with wave period 2.3s. Buoyancy acting on the tunnel per unit length equals 155kN, while the structural weight per unit length is 120kN. The buoyancy weight ratio (BWR, buoyancy/weight) of SFTP is 1.29. The configuration of tethers distribution is shown as Fig. 1(a). Four tilted tethers are located at the mid-span of tunnel and two pairs of vertical tethers are located at the 2nd and 4th tube segment. Tethers are consisted of steel wire with the outer diameter

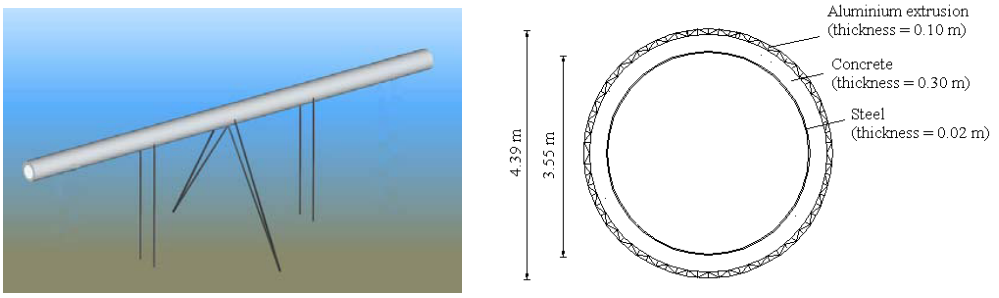

Fig. 1. (a) Schematic diagram of submerged floating tunnel prototype at Qiandao Lake; (b) Cross-section of tube segment

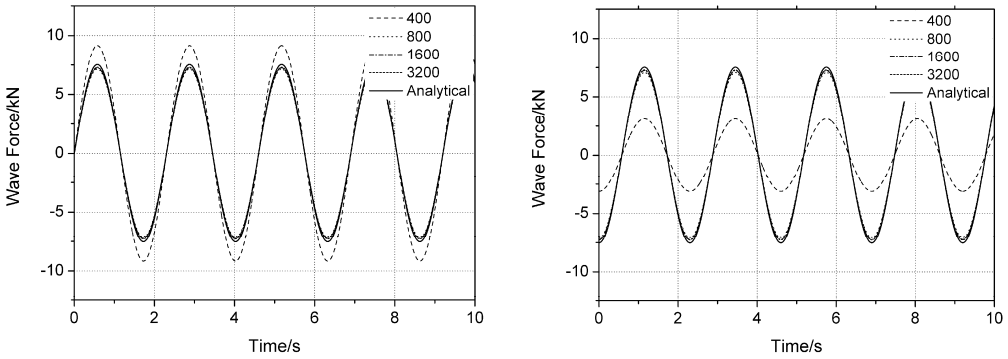

Fig. 2. Wave forces acting on the stationary tunnel with different amount of elements (a) Horizontal wave forces; (b) Vertical wave forces

Table 1. Natural frequencies of SFTP in air

Mode No.	Frequency(Hz)	Mode No.	Frequency(Hz)	Mode No.	Frequency(Hz)
1	1.57	8	11.87	15	28.17
2	2.30	9	14.22	16	29.08
3	4.28	10	14.25	17	35.23
4	4.59	11	20.78	18	36.12
5	8.66	12	20.86	19	36.13
6	8.74	13	23.54	20	44.57
7	9.69	14	28.15	21	44.60

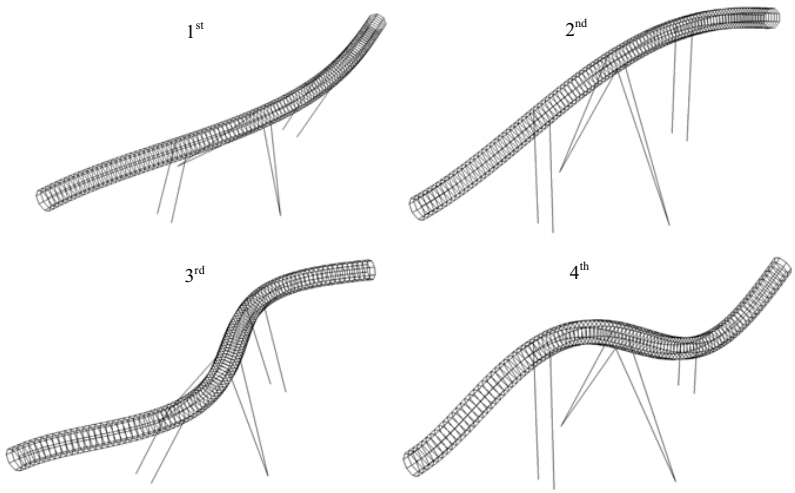

Fig. 3. Eigenmodes of SFTP

is 0.06m. Two ends of each tether are connected to the tunnel and the foundation individually with anchoring hock. The elastic module of tether is 140GPa and the broken tension force equals 3140kN for each tether.

Hydroelastic model of SFTP is formulated using mathematic method described as section 2. The hydroelastic dynamic equation for SFTP is the same as Eq. (20). The left hand of equation contains the fluid added mass and hydrodynamic damping, which are induced by the radiation wave due to the deflection of tunnel. The external forces on the right hand contain the diffraction wave force. The radiation wave potential and diffraction wave potential are both determined by solving Laplace equation (8) with boundary conditions (9~11). The only difference is the boundary condition (11), which is decomposed into Eq. (14) for each potential. The same method is adopted to solve the two potentials. Boundary elements are used to discretize the tunnel. Boundary integral equation for each element is formulated then the potentials are solved.

To verify the numerical program, a horizontal stationary tunnel is adopted to compute the wave force acting on it. This problem has analytical solution, which is compared to the numerical results with different amount of boundary elements. The comparison is presented as Fig. 2 containing the horizontal and vertical wave forces per unit length. When the number of elements exceeds eight hundred, the numerical result approximates the analytical solution very closely. Considering the more elements used the more time consumed by computation, we adopted eight hundred elements to discretize the tunnel. Eight elements are used along the circumference of tunnel cross-section, one hundred elements are distributed along the tunnel axle.

The natural frequencies and corresponding eigenmodes are presented by solving Eq. (2). To keep the consistency with the boundary elements, the same amount of finite elements are adopted. General software ABAQUS is used to solve the eigenvalue of SFTP. From the mode decomposition point of view, the number of reserved mode must make sure the ratio of effective mass to total mass on each degree of freedom exceeds 90%. Here twenty one modes are used to simulate the response of SFTP. Table 1 shows the natural frequencies of SFTP in air. The first four eigenmodes are presented in Fig. 3. In the finite element model, the sandwich structure of SFTP has been simplified into a uniform shell with equivalence density is 2125.8kg/m^3, elastic module is $3.2\times10^{10}\text{N/m}^2$ and the effective inner diameter of tunnel is 3.53m [9]. Here, these values are deduced by the bending stiffness, gravity and buoyancy equivalence principles.

4. Results and discussion

The tunnel tubes are discretized into shell elements not as beam elements. It is necessary to present the distributions of deflection or stress in the cross-section of tunnel. In the prototype design, at one tunnel end, there is a stress relaxation device to absorb the axial deflection energy of tunnel. This device is important for the safety of tunnel considering the deformation of tunnel due to earthquake, wave, thermal stress etc. However, from the symmetry of structure point of view, one stress relaxation device at each tunnel end may be a more optimized design for the tunnel deflection, although this would increase the cost of SFTP.

Based on the hydroelastic model of SFTP described in the previous section, for comparison, the dynamic response of two models with different tunnel end connectors are simulated. Model A contains only one stress relaxation device at the right tunnel end. At the other tunnel end three translational degrees of freedom are constrained. Model B contains one stress relaxation device at each tunnel end. Fig. 4 to 6 shows the tunnel deflection along the three translation degrees of freedom individually. The instantaneous deflections of tunnel are presented at the time when the horizontal deflection reaches the maximum. The ratio of length to diameter of tunnel has been adjusted for more convenient drawing.

The deflection of Model B is obviously more symmetric compared to Model A. Due to the existence of axial stress relaxation device at each tunnel end in Model B, more flexible of tunnel induces the larger deflection occurs except at the horizontal direction. The relaxation device influences directly the axial response of tunnel, therefore the difference of axial deflection is the largest compared to the other two translational deflections. For Model B, the maximum axial deflection occurs in the cross-section at the tunnel end. The maximum deflections along horizontal and vertical directions both occur in the cross-section at the mid-span. However for Model A, the maximum deflections are prone to occur deviating from mid-span to the tunnel right end where there is the relaxation device. Here the vertical deflection of tunnel contains the contribution from the net buoyancy. Comparing with horizontal deflection, one could conclude that wave forces acting on the tunnel are far smaller than net buoyancy. The deflections of tunnel induced by wave forces are the same order of millimeters for both models.

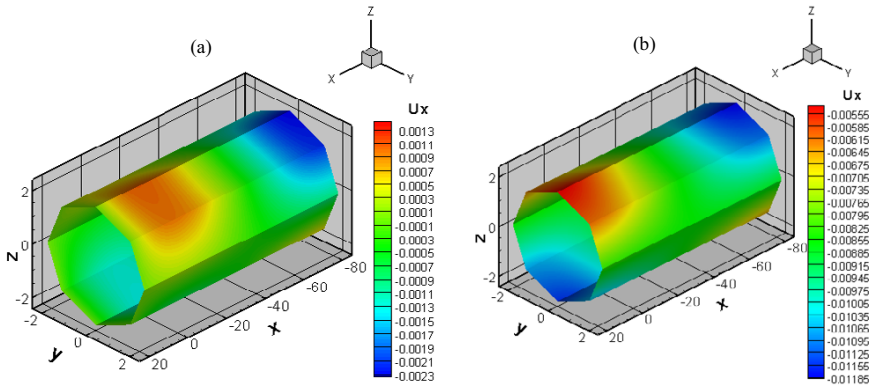

Fig. 4. Distribution of axial deflection along the tunnel: (a) Model A; (b) Model B (unit: m)

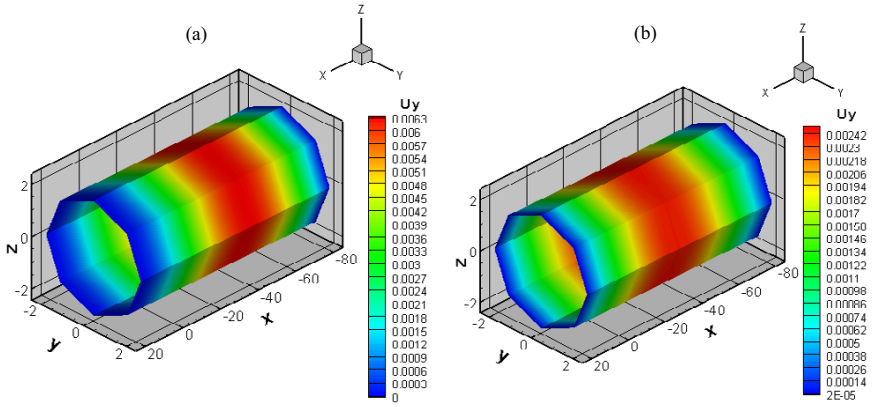

Fig. 5. Distribution of horizontal deflection along the tunnel: (a) Model A; (b) Model B (unit: m)

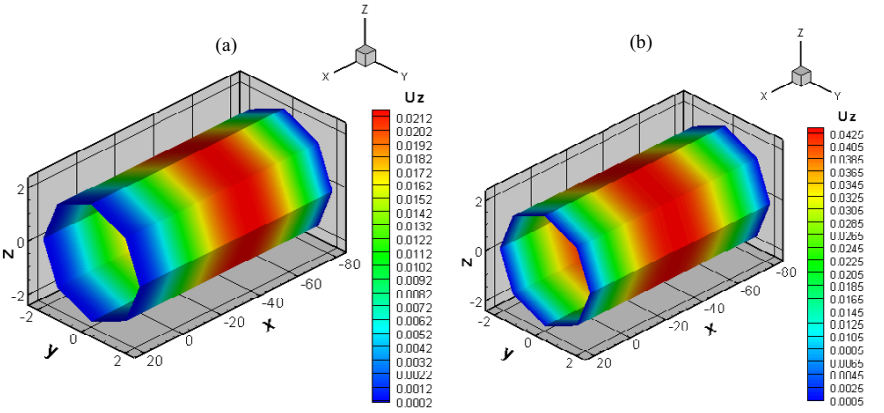

Fig. 6. Distribution of vertical deflection along the tunnel: (a) Model A; (b) Model B (unit: m)

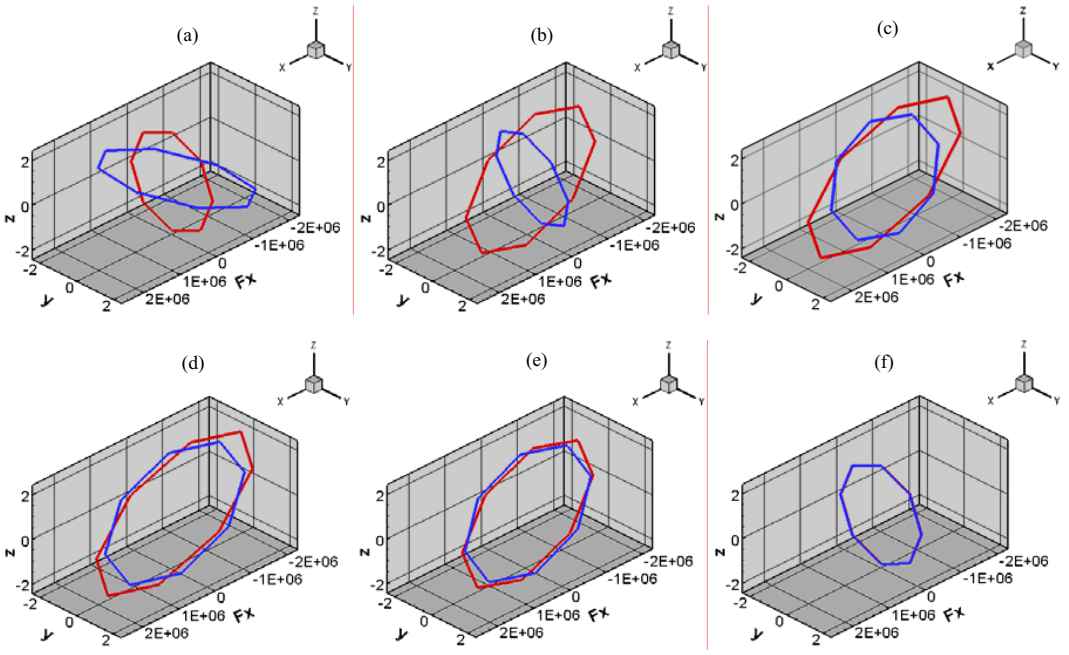

Fig. 7. Distribution of axial membrane force along the cross-section of each connector (a) left tunnel end connector; (b) 1st tube segment connector; (c) 2nd tube segment connector; (d) 3rd tube segment connector; (e) 4th tube segment connector; (f) right tunnel end connector. Blue line represents Model A and red line represents Model B (Unit of Fx: N)

Connectors between tube segments are full strength connections for both models. The simulation results show that axial membrane force is dominant in each connector compared to shear forces. Usually axial membrane force is larger one or two order of magnitude than shear force in connector. Fig. 7 shows the distribution of axial membrane force along the cross-section of each connector including tunnel end connectors. For Model A, represented by blue line in Fig. 7, the maximum axial membrane force occurs at the left tunnel end connector. At the other tunnel end connector, due to the existence of stress relaxation device, axial force equals zero. For Model B, represented by red line in Fig. 7, axial membrane forces at both tunnel end connectors equal zero. However, axial membrane force at each tube segments connector is larger than the corresponding connector in Model A, especially for the 1st and 2nd connectors. Due to the symmetry of Model B, axial membrane forces at different tube segment connectors have the similar distributions.

5. Conclusions

This paper presents a hydroelastic model of SFT considering the fluid-structure interaction under wave condition. Due to the elasticity of SFT, deflection and motion of structure induce the radiation wave propagating. Fluid added mass and hydrodynamic damping are necessary to be taken into account, which are functions of structural acceleration and velocity. Boundary element and structural mode decomposition methods are adopted to solve radiation wave potentials. Dynamic equation of SFT is solved in frequency domain. As a case study, we simulated the response of SFTP due to wave forces at Qiandao Lake using hydroelastic analysis method. Using the different tunnel end connectors, the distribution of tunnel defection and axial forces at connectors are compared. Under the wave condition at Qiandao Lake, deflections of SFTP are only at the same order of millimeters weather stress relaxation device is used in tunnel end connectors or not. If only one stress relaxation device is used in either tunnel end connector, the maximum axial membrane force occurs at the other end connector. However, if stress relaxation device is used in each tunnel end connector, the axial membrane forces will increase at each tube segment connector.

Acknowledgements

This paper is supported by National Natural Science Foundation of China (nos. 10532070, 10772178) and Knowledge Innovation Program of Chinese Academy of Sciences (no. KJCX2-YW-L07).

References

[1] Ahrens D. Submerged floating tunnels: A concept whose time has arrived. *Tunn Undergr Space Technol* 1996; 11: 505–510.

[2] Wu Y. *Hydroelasticity of Floating Bodies*. UK: Brunel University; 1984.

[3] Price WG, Wu Y. Hydroelasticity of marine structures. *16th International Congress of Theoretical and Applied Mechanics (IUTAM)*, Denmark: Sectional Lecture; 1985, S-10.

[4] Bishop RED, Price WG, Wu Y. A general linear hrdroelasticity theory of floating structures moving in a seaway. *Phil Trans R Soc London* 1986; A316: 375-426.

[5] Newman JN. Wave effects on deformable bodies. *Applied Ocean Research* 1994; 16: 167-185.

[6] Cui W, Yang J, Wu Y, Liu Y. *Theory of Hydroelsticity and Its Application to Very Large Floating Structures*. 1st ed. Shanghai: Shanghai Jiao Tong University; 2007.

[7] Fiorentino A, Mazzolani FM, Perotti F, et al. (Italian Team of SIJLAB). Design report of the Archimede's bridge prototype in Qiandao Lake (P.R of China). Italy, 2007.

[8] Hong Y, Li J. Liang N, Ge F, Huang G, Gao F, Lin M, Chen W, et al. (Chinese Team of SIJLAB). Report of research and design for Archimedes bridge prototype at Qiandao Lake. Institute of Mechanics, CAS, 2007.

[9] Long X, Ge F, Wang L, Hong Y. Effects of fundamental structure parameters on dynamic response of submerged floating tunnel under hydrodynamic loads. *Acta Mech Sinica* 2009; 25: 335-344.